Reduced Chemical Kinetics for the Modeling of TiO$_2$ Nanoparticle Synthesis in Flame Reactors

Maulik Mehta,[‡] Rodney O. Fox,[‡] and Perrine Pepiot*,[§]

[‡]Department of Chemical and Biological Engineering, Iowa State University, Ames, Iowa 50011, United States
[§]Sibley School of Mechanical and Aerospace Engineering, Cornell University, Ithaca, New York 14853, United States

S *Supporting Information*

ABSTRACT: Flame synthesis represents a viable technique for large-scale production of titanium dioxide (TiO$_2$) nanoparticles. A key ingredient in the modeling of this process is the description of the chemical kinetics, which include Ti oxidation, hydrocarbon fuel combustion, and chlorination. While detailed chemical mechanisms have been developed for predicting TiO$_2$ nanoparticle properties by West et al. (e.g., *Combust. Flame* **2009**, *156*, 1764), their use in turbulent reacting flow simulations is limited to very simple configurations or requires significant modeling assumptions to bring their computational cost down to an acceptable level. In this work, a reduced kinetic scheme describing the oxidation of TiCl$_4$ in a methane flame is derived from and validated against the predictions of a detailed mechanism from the literature. The reduction procedure uses graph-based methods for unimportant kinetic pathways elimination and quasi-steady-state species selection. Reduction targets are chosen in accordance with previous modeling results that showed the importance of temperature and overall concentration of titanium-containing species in both nucleation and surface growth rates. The resulting reduced scheme is thoroughly evaluated over a wide range of conditions relevant to flame-based synthesis, and the capability of the reduced model to adequately capture the process dynamics at a much lower computational cost is demonstrated.

INTRODUCTION

Flame-based synthesis is the preferred method for the industrial level production of commercial grade metal—oxide nanoparticles and, hence, is the chosen technique for production of titania (TiO$_2$) nanoparticles. Titanium dioxide nanoparticles are traditionally used as white pigments but have found use in diverse areas like photocatalysis,[1] reducing nitrogen oxide emissions,[2] catalyst supports,[3] ultraviolet filtering materials,[4] surface treatments like antifog coating,[5] or cosmetics.[6] Despite the industrial importance of titanium dioxide and predicted rise in market revenues,[7] the chemistry and flow dynamics at the core of TiO$_2$ flame synthesis are not well understood, and process optimization remains mostly empirical. The development of predictive computational models offers an attractive avenue to gain a better insight into the synthesis process and devise strategies to achieve a tighter control over the resulting particle properties.

In the flame synthesis of titania nanoparticles, the precursor TiCl$_4$ is oxidized to form TiO$_2$. Typically, a hydrocarbon-based fuel like methane (CH$_4$) is used in the reactor to support the flame and provide the high temperatures needed for titanium (Ti) oxidation. To predict the properties of nanoparticles synthesized in flame-based reactors, computational models have to adequately capture the complexity of the corresponding chemical processes, including the coupling between nanoparticles and hydrocarbon oxidation in the flame, the transition from the gas-phase species to the particulate phase, and the subsequent particle evolution (i.e., nucleation and surface growth).[8] Previous work[9,10] has shown that the gas-phase chemical mechanism used in the model can potentially play an important role in determining the nucleation dynamics and subsequent surface growth. Indeed, simulations that use the

detailed gas-phase kinetic mechanism developed by West et al.[11,12] yield significantly different results compared to one-step models that forego Ti intermediates entirely. For example, when coupled with a population balance approach containing nucleation, growth, aggregation, and sintering terms, detailed chemical models yield two different regimes:[10] an initial nucleation-dominated regime, in which gas-phase reactions mostly lead to nucleation, and a surface-growth regime occurring later in the synthesis process, where surface reactions dominate. In contrast, for the same flow conditions,[10] the one-step model predicts nucleation due to complete consumption of the TiCl$_4$, followed by aggregation.

The differences between the detailed and single-step chemistry models have been investigated in idealized, low-dimensional configurations such as multienvironment plug flow (PFR) or partially stirred reactors (PaSR),[10] for which large kinetic schemes are computationally affordable. However, computational fluid dynamics (CFD)-based methods will be needed to capture the effects of mixing and turbulence on product properties more accurately than simple flow models. CFD methods are significantly more expensive, especially when the chosen combustion models rely on finite-rate chemistry, which requires the solution of many transport equations for the chemical species, and are thus limited in terms of the number of chemical species they can afford. In particular, the relatively large sizes of the detailed chemical models used so far (up to

107 species[10]) prohibit their direct use in CFD, that is, without resorting to equilibrium or flamelet models.[13]

Starting from the detailed mechanism of West et al.,[11] the objective of this work is therefore to develop a reduced mechanism to describe the gas-phase chemical kinetics of relevance for titania formation that retains an accurate description of the most important chemical pathways and Ti intermediates contained in the detailed mechanism, small enough to be of practical use in turbulent combustion frameworks based on finite-rate chemistry (for example Large-Eddy Simulation/Probability Density Function (LES/ PDF) approaches,[14] which can efficiently handle up to a few dozen chemical species.[15])

Numerous techniques have been developed to drastically reduce the computation burden associated with detailed chemistry description. A nonexhaustive list includes: (i) automatically generated skeletal mechanisms through negligible species and reaction elimination;[16−22] (ii) dimension reduction techniques, which further decrease the number of species or degrees of freedom that need be considered, including chemical lumping,[23,24] mathematical lumping,[25] Quasi-Steady-State Assumptions (QSSA),[26,27] Rate Controlled Constrained Equilibrium (RCCE),[28] Intrinsic Low Dimension Manifold (ILDM),[29] Reaction Diffusion Manifolds (REDIM),[30] and Invariant Constrained Equilibrium Edge PreImage Curve (ICE-PIC);[31] and (iii) storage/retrieval algorithms to reduce the computational cost of repetitive kinetics calculations, including In-Situ Adaptive Tabulation (ISAT)[32] and Piecewise Reusable Implementation of Solution Mapping (PRISM).[33] Rather than being in competition, these general approaches can be used in combination with a compounding of the benefits.

In this work, we use the Directed Relation Graph with Error Propagation (DRGEP) method[18] to eliminate unimportant chemical pathways from the chemical description and replace appropriate species differential equations with quasi-steady state approximations. With the detailed mechanism taken as reference, DRGEP uses an error propagation algorithm to quantitatively estimate the role of each species and reaction in predicting a user-defined set of targets, thereby identifying the most important reaction pathways. To be efficient, the algorithm must be applied to a large number of gas compositions (or chemical snapshots) of potential relevance to the simulations of interest. Here, partially stirred reactor (PaSR) simulations, as described for example in Ren and Pope,[34] are used to densely and conservatively sample the composition space in regions potentially relevant for more complex flame simulations. The same PaSR configurations are also used to assess the accuracy of the resulting reduced models through comparisons with predictions obtained with the reference detailed mechanism.

This article is organized as follows: the reference detailed kinetic mechanism,[11,12,35,36] as used in previous work[10] to model flame synthesis of titania, is first described in the "Detailed Chemical Description" section, followed by a description of the PaSR configuration used here to develop and validate reduced chemical models. The main features of the DRGEP reduction technique and its application to the PaSR configuration are then discussed in the "Model Reduction" section, followed by a detailed account of the species and reaction elimination process and the selection of quasi-steady state species, done with extensive error quantification. A brief analysis of the chemical pathways retained in the reduced model concludes that section.

■ DETAILED CHEMICAL DESCRIPTION

The detailed kinetic mechanism that serves as reference in this work has been obtained by combining three different submechanisms for methane oxidation,[35] TiCl$_4$ oxidation,[11,12] and hydrocarbon chlorination,[36] as illustrated in Figure 1.
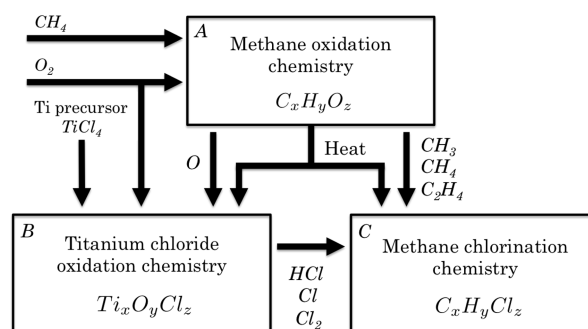

Figure 1. Kinetic submechanisms included in the detailed chemistry description and main coupling chemical species. References for each submechanism are A,[35] B,[9,11,12] and C.[36]

Detailed chemical kinetics for TiCl$_4$ oxidation have been developed by West et al.[11,12] using density functional theory (DFT) based quantum calculations. The resulting mechanism contains 30 species and 66 reversible reactions to describe the Ti oxidation process. In contrast to one-step approaches that consider only the overall reaction,

$$TiCl_4 + O_2 \rightarrow TiO_2 + 2Cl_2 \tag{1}$$
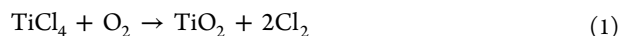
the detailed kinetics include a large number of intermediate species of the form Ti$_x$O$_y$Cl$_z$ that undergo reactions such as thermal decomposition, radical abstraction and disproportionation, oxidation, and dimerization. To describe nanoparticle formation for the detailed mechanism proposed by West et al.,[12] three nucleation reactions were added by Mehta et al.[9]

In a flame, the Ti oxidation process is expected to be more complicated, as interactions between fuel, precursor, and oxidizer become significant and need to be taken into account. The main purpose of the flame is to provide heat to initiate the endothermic TiCl$_4$ decomposition reactions (reactions R1, R2, and R3 in Table 1 of West et al.[11]) leading to Ti oxides. Methane (CH$_4$) is typically used as the hydrocarbon fuel, and its combustion is described here using the GRI-Mech 2.11 mechanism.[35] Finally, the oxidation of TiCl$_4$ to form TiO$_2$ leads to the formation of chlorine gas, Cl$_2$. The presence of Cl$_2$ can lead to hydrocarbon chlorination; therefore, the methane chlorination chemistry described in Shah and Fox[36] is added to the full kinetic scheme.

In summary, the chemical mechanism used in this work contains 107 species and 1007 reactions (forward and backward counted separately) to describe Ti oxidation in a methane flame. Details on the individual reactions included in this kinetic scheme can be found in the cited literature.[9,12,35,36] This mechanism has been analyzed in previous work[9,10] and its performances compared qualitatively to experimental data and one-step kinetics results. Undoubtedly, future improvements will be needed in the detailed mechanism to capture the coupling between gas-phase and surface reactions[37] and to improve agreement with experiments. In this work, as our objective is to validate the accuracy of the reduced mechanisms relative to the detailed mechanism, predictions of the reduced

mechanisms are compared to those of the detailed chemical mechanism and not to experimental data.

SIMULATION CONFIGURATION

Partially Stirred Reactor. The idealized partially stirred reactor (PaSR) is used here as the test configuration to extract a reduced-order chemical model from the detailed, 107-species mechanism described above. Inside a PaSR reactor, reaction occurs and the mean thermochemical properties are assumed to be statistically spatially homogeneous, but the fluid is imperfectly mixed at the molecular level. As such, the PaSR can be seen as a computationally inexpensive representation of a single grid cell embedded in a large simulation of turbulent combustion and is designed to access the broadest possible range of compositions of potential relevance for more complex flame simulations.

The reacting ideal gas-phase mixture, consisting of n_s chemical species, is assumed to evolve in the PaSR at a fixed pressure p, so that the full thermochemical state, or composition, of the mixture Φ is completely characterized by the n_s vector of species mass fractions $\mathbf{Y}$ and the mixture temperature T: $\Phi \equiv \mathbf{Y}, T$, or equivalently, the species mass fractions $\mathbf{Y}$ and the mixture enthalpy h: $\Phi' \equiv \{\mathbf{Y}, h\}$. The temperature being easily obtained from enthalpy (and conversely), both representations can be used interchangeably. The PaSR is continuously fed by a user-determined number n_{str} of inflow streams of prescribed compositions Φ_{str}. The reactor contains a constant, even number n_p of particles, the nth particle having a composition $\Phi^{(n)}$. Those compositions evolve in time by increment Δt due to mixing, reaction, and inflow and outflow events.

In the inflow/outflow event, n_{in} particles are selected at random with equal probability, and their compositions are replaced by inflow stream compositions. The integer number n_{in} and the inflow compositions are chosen according to the user-specified mean residence time τ_{res} and streams mass flow rates $\dot{m}_{str}^{k=1\ldots n_{str}}$, respectively. Note that inflow and outflow events change the particle compositions in a discontinuous manner. In contrast, reaction and mixing change the particle compositions continuously and are treated as two fractional steps with an operator-splitting scheme. In the mixing fractional step, particles are paired and ordered so that particles n and $n + 1$ are partners for odd n ($1 \leq n < n_p$). The compositions after the mixing fractional step of partners n and $n + 1$ are computed from the enthalpy-based compositions at time t as

$$\Phi'^{(n),m} = \Phi'^{(n)}(t) - \frac{\Delta t}{\tau_{mix}}(\Phi'^{(n)}(t) - \Phi'^{(n+1)}(t))$$

$$\Phi'^{(n+1),m} = \Phi'^{(n+1)}(t) - \frac{\Delta t}{\tau_{mix}}(\Phi'^{(n+1)}(t) - \Phi'^{(n)}(t)) \quad (2)$$

where τ_{mix} is the specified time scale for the pairwise mixing. At each time step, n_{pair} particles are selected randomly with equal probability and shuffled to change partners. The integer number n_{pair} is chosen according to a user-specified pairing time τ_{pair}, typically taken equal to τ_{mix}. The compositions after mixing are converted back to their temperature representations $\Phi^{(n),m}$, which then evolve under isobaric, adiabatic conditions over a time Δt according to

$$\frac{d\Phi^{(n),m}(t)}{dt} = \mathbf{S}(\Phi^{(n),m}(t)) \quad (3)$$

where $\mathbf{S}$ is the chemical source term defined by the user-provided kinetic reaction mechanism, consisting of n_r reactions. This reaction fractional step finally yields the particle compositions at $t + \Delta t$: $\Phi^{(n)}(t + \Delta t)$.

Conditions and Parameters. The partially stirred reactor as described above serves two purposes in this work: First, it allows us to quickly assemble a large set of sample diverse compositions potentially relevant for TiO_2 synthesis in methane flame, a necessary prerequisite to apply the DRGEP chemistry reduction technique. Second, it provides an ideal setting to directly assess the ability of the generated reduced kinetic models to reproduce the dynamics of the full chemical scheme along a wide range of chemical trajectories, thereby ensuring that all potentially important reaction pathways are retained. Previous work[10] has shown that inflow conditions play a major role in determining the size and shape of titanium oxide particles. Therefore, two different configurations will be studied here. The first one, premixed in nature, injects mixtures of $TiCl_4$ and air, and CH_4 and air, while the second one is essentially nonpremixed, with $TiCl_4$ and methane being injected separately from the oxidizer. Those configurations are representative of Flames A and D in the experimental work of Pratsinis et al.[3] and will therefore be labeled PaSR−A and PaSR−D, respectively. The full list of parameters for PaSR−A and −D is provided in Table 1.

DIRECTED RELATION GRAPH WITH ERROR PROPAGATION (DRGEP)

To significantly accelerate the development of an appropriate reduced chemical model, the automatic chemistry reduction

Table 1. PaSR−A and −D Simulation Parameters

Reactor Characteristics	
residence time	0.01 s
mixing time	10^{-3} s
pairing time	10^{-3} s
time step	10^{-4} s
number of particles	100

Initial Conditions	
temperature	2500 K
pressure	1 bar
N_2 (mass fraction)	1

Inflow Conditions: PaSR−A			
parameters	stream 1	stream 2	stream 3
normalized streamflow rates	0.4721	0.1542	0.3537
temperature	333 K	1450 K	298 K
Ar (mass fraction)	0.08	0	0
CH_4 (mass fraction)	0	0.185	0
N_2 (mass fraction)	0.686	0.605	0.767
O_2 (mass fraction)	0.209	0.21	0.233
$TiCl_4$ (mass fraction)	0.025	0	0

Inflow Conditions: PaSR−D			
parameters	stream 1	stream 2	stream 3
normalized streamflow rates	0.1370	0.0026	0.8604
temperature	333 K	1100 K	450 K
Ar (mass fraction)	0.55	0	0
CH_4 (mass fraction)	0.278	0.026	0
N_2 (mass fraction)	0	0.512	0.767
O_2 (mass fraction)	0	0.155	0.233
$TiCl_4$ (mass fraction)	0.167	0.327	0

technique DRGEP (Directed Relation Graph with Error Propagation) is used.[18] By analyzing production rates derived from an ensemble of composition states, the method quantifies the coupling between the species and reactions involved in a chemical mechanism and a set of user-specified targets. The main output from this analysis is a set of importance coefficients, which will be referred to as DRGEP coefficients, allowing us to rank species and reactions from most important to least important for the prediction of the chosen targets. Species and reactions with the lowest coefficients are then removed from the mode. The main steps of the DRGEP method are detailed below in the context of TiO_2 synthesis in a methane flame.

Reduction Targets. The first step of the DRGEP method is to identify a set of n_T targets $\mathcal{T}$, most often specific species or heat release, that the reduced model will have to reproduce accurately. In TiO_2 synthesis, we are especially interested in the prediction of O_2 and nuclei precursor concentrations, in this case, $Ti_5O_6Cl_8$, both included as DRGEP targets, since they will determine the nucleation rate:

$$J = k_{nucl} N_{av} [Ti_5O_6Cl_8][O_2]^2 \qquad (4)$$

where the pre-exponential factor is $k_{nucl} = 10^{13}$ m^6/(mol^2·sec) and N_{av} is the Avogadro number.[9] It was shown by Mehta et al.[10] that detailed surface growth models, which involve all $Ti_xO_yCl_z$ intermediates in the calculation of the surface growth source terms, significantly improve the description of TiO_2 nanoparticle synthesis. Therefore, both $TiCl_4$ and the sum of all $Ti_xO_yCl_z$ species mass fractions are added to the reduction targets set. Finally, since the synthesis process is highly sensitive to temperature, and according to common practices in DRGEP-based reduction,[18] heat release and CO mass fraction are also added to ensure that the reduction procedure retains an appropriate description of the methane oxidation process.

Sample Compositions Database. To evaluate the relative importance of species and reactions for the set of targets, DRGEP requires an ensemble of sample compositions $\mathcal{D}$ representative of the simulations in which the reduced model is going to be used eventually. We assume here that particles in a PaSR simulation with inflow conditions matching the turbulent flames of interest will follow trajectories in composition space that are close to those they would encounter in the actual flame, an assumption commonly done when deriving reduced models for turbulent flame simulations.[38] Therefore, we randomly sample compositions encountered in the two PaSR test configurations, PaSR−A and −D, until we have a database large enough to encompass all relevant chemical processes and dynamics. The database used in this work consists of 20 000 distinct chemical compositions.

DRGEP Importance Coefficients. Once an appropriate sample composition database has been obtained, each sample is analyzed by the DRGEP methodology to quantify the importance of species and reaction, first at the individual sample level and then for the overall chemical process. A brief summary of how the importance coefficients are computed is provided next.

- **Direct interaction coefficients.** Direct interaction coefficients are defined as the measure of the coupling between two species that are **directly** related through an elementary reaction, that is, two species that appear concurrently in the same reaction. The coupling coefficient between two such species A and B for a given composition Φ is expressed as

$$r_{AB} \equiv \frac{|\sum_{i=1,n_R} \nu_{i,A} \omega_i \delta_B^i|}{\max(P_A, C_A)} \qquad (5)$$

where the production and consumption of species A are defined as

$$P_A = \sum_{i=1,n_R} \max(0, \nu_{i,A} \omega_i) \qquad (6)$$

$$C_A = \sum_{i=1,n_R} \max(0, -\nu_{i,A} \omega_i) \qquad (7)$$

In the above equations, ω_i are the net reaction rate of the ith reaction evaluated from composition Φ and the detailed chemical model, $\nu_{i,A}$ is the stoichiometric coefficient of species A in reaction i, and

$$\delta_B^i = \begin{cases} 1 & \text{if the } i\text{th reaction involves species B} \\ 0 & \text{otherwise} \end{cases} \qquad (8)$$

- **Path-dependent coefficients.** To go beyond direct interactions, DRGEP defines path-dependent coefficients that quantify the coupling between any directly or indirectly related species A and B. Assuming geometric damping, and again, for a given composition Φ, the coupling between A and B through a reaction path p is written as

$$r_{AB,p} = \prod_{i=1}^{n-1} r_{S_i S_{i+1}} \qquad (9)$$

with $S_1 = A$, $S_n = B$, S_i being on the reaction path p that links A and B, n being the number of reactions involved in path p. Because many paths can exist linking A to B, only the most important one is retained:

$$R_{AB} \equiv \max_{\text{all paths } p} r_{AB,p} \qquad (10)$$

R_{AB} can be interpreted as the magnitude of the error made in the prediction of species A if species B is removed.[18]

- **Target-specific coefficients.** In a similar way, the overall importance of B to the target set $\mathcal{T}$ for a given composition Φ is defined by

$$R_{B,\Phi} \equiv \max_{\text{all targets } T} R_{TB} \qquad (11)$$

- **Extension to multiple composition states.** The above results can be extended to any given ensemble of compositions $\mathcal{D}$ to yield the DRGEP importance coefficient of species B over $\mathcal{D}$:

$$R_B^{\mathcal{D}} = \max_{\Phi \in \mathcal{D}} R_{B,\Phi} \qquad (12)$$

A similar procedure can be derived to calculate an importance coefficient of any reaction r, $R_r^{\mathcal{D}}$. For additional details, the reader is referred to Pepiot and Pitsch.[18] In the following, we will refer to the n_S-vector of species importance coefficients over database $\mathcal{D}$ as $\mathbf{R}^{\mathcal{D},S}$, the ith element corresponding to the ith species in the mechanism, and to the n_R-vector of reaction
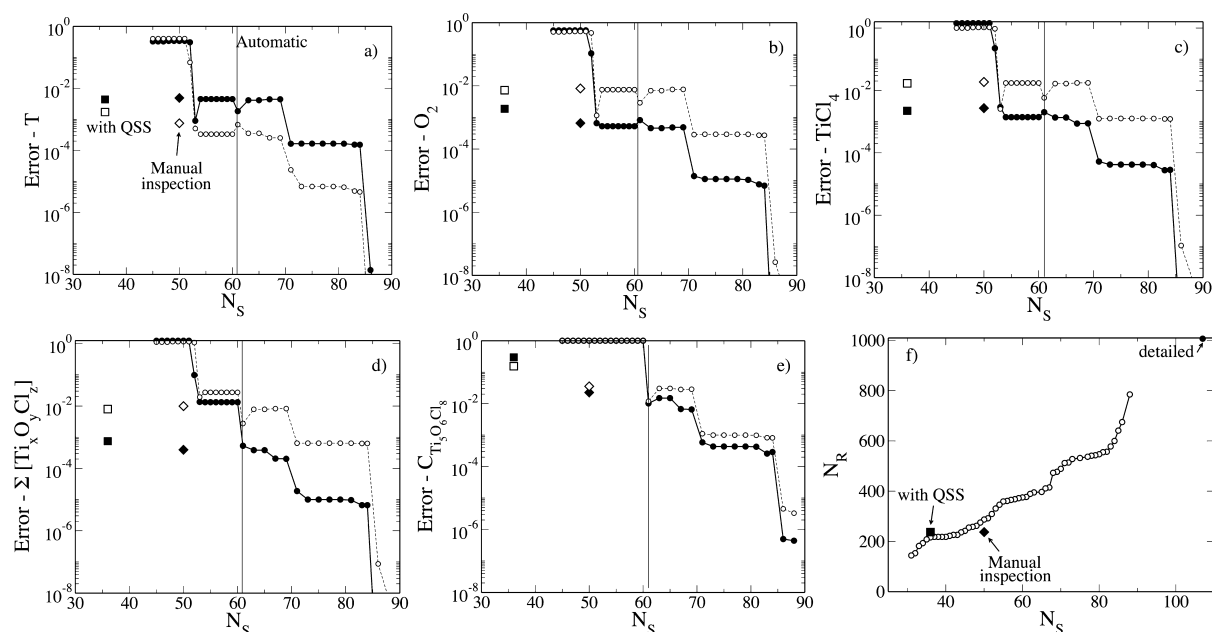
Figure 2. Error in PaSR predictions as a function of the number of species retained in the skeletal model during reduction: (a) temperature, (b) O_2, (c) $TiCl_4$, (d) $\sum[Ti_xO_yCl_z]$, (e) nucleation rate evaluated from $Ti_5O_6Cl_8$ consumption rate (eq 4), and (f) number of reactions retained in the model. Filled symbols: PaSR−A; open symbols: PaSR−D. Circles: automatic reduction; diamonds: manual inspection of the 61-species automatically generated mechanism; squares: with quasi-steady state assumption.

importance coefficients as $\mathbf{R}^{\mathcal{D},\mathcal{R}}$, the jth element corresponding to the jth reaction in the mechanism.

MODEL REDUCTION

Automatic Reduction and Error Evaluation Procedure. The automatic reduction procedure proceeds through two distinct steps. In the first one, a list of kinetic models of decreasing complexity, is established a priori using the DRGEP methodology. In contrast to previous use of DRGEP, however, species and reaction eliminations are combined in a single step thanks to an a priori error estimate on production rates. This step is carried out on the sample database itself and does not involve any PaSR simulations, which keep the computational cost to a minimum. The details of the algorithm are provided below. In this algorithm, $S_T^{(n),D}$ and $S_T^{(n),R}$ are the chemical source terms evaluated for sample (n) in the database with the full model and the ACTIVE part (species and reaction) of the model, respectively.

Algorithm 1 Species and reaction elimination algorithm

1: Start with all species and reactions set as ACTIVE
2: $k = 1$
3: **for** $i = 1$ to n_S **do**
4:     Compute DRGEP species coefficients $\mathbf{R}^{\mathcal{D},S}$ for all ACTIVE species
5:     Sort $\mathbf{R}^{\mathcal{D},S}$ by increasing value
6:     Set status of species i with lowest $R_i^{\mathcal{D},S}$ coefficient to INACTIVE.
7:     Set reactions involving species i to INACTIVE
8:     Evaluate a priori target error as $\tilde{\varepsilon} = \max_{\mathcal{T}}\left(\sum_{\mathcal{D}}|S_T^{(n),D} - S_T^{(n),R}|/\sum_{\mathcal{D}}|S_T^{(n),D}|\right)$
9:     $\tilde{\varepsilon}_S \leftarrow \tilde{\varepsilon}$
10:     Compute DRGEP reaction coefficients $\mathbf{R}^{\mathcal{D},R}$ for all ACTIVE species and ACTIVE reactions.
11:     **while** $\tilde{\varepsilon} \leq \tilde{\varepsilon}_S$ **do**
12:         Set status of reaction j with lowest $R_j^{\mathcal{D},R}$ coefficient to INACTIVE.
13:         Re-evaluate $\tilde{\varepsilon}$
14:     Store all ACTIVE reactions and species as model k
15:     $k \leftarrow k + 1$

In the second stage, the test configurations PaSR−A and PaSR−D are simulated using each of the reduced models generated in the first stage, and a posteriori (actual) errors on targets are computed, defined for any target T as

$$\varepsilon_T = \frac{\int_0^{t_{\text{end}}} |\langle T \rangle^R(t) - \langle T \rangle^D(t)| \, dt}{\int_0^{t_{\text{end}}} |\langle T \rangle^D(t)| \, dt} \tag{13}$$

In this equation, $\langle T \rangle(t)$ designates the average at time t of quantity T over all particles contained in the PaSR, and t_{end} is taken here as 15 PaSR residence times. Those errors are plotted as a function of the number of species retained in the model for both PaSR conditions for temperature (Figure 2a), O_2 (Figure 2b), $TiCl_4$ (Figure 2c), $\sum[Ti_xO_yCl_z]$ (Figure 2d), and nucleation rate evaluated as the consumption rate of precursor $Ti_5O_6Cl_8$, provided by eq 4 (Figure 2e), while Figure 2f shows how the number of reactions varies as the number of species decreases. For all targets, we observe a mostly monotonic increase of errors as the number of species is reduced, until the reduction becomes so severe that errors become of order 1. The 61-species mechanism, indicated in all graphs by a vertical line, is the smallest acceptable model generated by the DRGEP procedure: past this model, $Ti_5O_6Cl_8$ consumption rate errors become unacceptably large.

Additional Reduction. *Manual Inspection.* To complement the automatic procedure, the 61-species mechanism obtained above is further reduced using sensitivity analysis and reaction pathways analysis. A semiautomatic procedure is used, in which a set of additional species and reactions that could be potentially removed is provided by the user. Appropriate mechanisms are then generated and errors automatically computed (eq 13). The user is then prompted to accept or reject the additional species and reactions eliminations. An additional 10 species are removed through this step, and the corresponding errors on targets are indicated as diamonds in Figure 2.

QSS Assumptions. To increase the speed up of the skeletal mechanism obtained through species and reaction elimination, quasi-steady state assumptions are introduced that replace part of the differential equations by algebraic equations, which are

much faster to evaluate. The methodology of Pepiot[39] is used, in which a steady state parameter $R_{QSS, B}$ is introduced to quantify the suitability of a given species B to be set in steady state:

$$R_{QSS,B} = \max_{\Phi \in D}(R_{B,\Phi}^S [B]_\Phi \tau_{B,\Phi})$$ (14)

where

$$\tau_{B,\Phi} = -\left[\frac{\partial(P_{B,\Phi} - C_{B,\Phi})}{\partial[B]_\Phi}\right]^{-1}$$ (15)

The R_{QSS} values of species retained in the 51-skeletal model are plotted in Figure 3. While all species with low R_{QSS} are typically
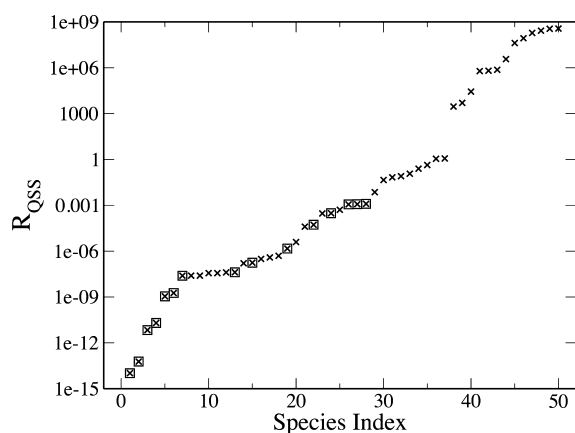
Figure 3. Steady state coefficients for each species retained in the skeletal model (×). Squares indicate species set in quasi-steady state in the final model.

suitable QSS species, we add an additional constraint that the resulting algebraic system to evaluate the concentrations of the QSS species remain linear. With this constraint, 15 species are set in steady state, namely: $CH_2(S)$, CH_2, CH, C_2H_3, TiO_2Cl_2, HCO, CH_3O, $Ti_3O_4Cl_4$, C_2H_5, CH_2Cl, $CHCl_2$, CH_2Cl_2, $CHCl_3$, H_2O_2, and $Ti_2O_3Cl_3$. Those species are indicated by an extra square in Figure 3.

Final Reduced Model. The final model consists of 36 species (including inert nitrogen and argon), 15 quasi-steady state species, and a total of 237 reactions, forward and backward counted separately. Error levels are small, of the order of 1% for all targets, except for $Ti_5O_6Cl_8$ consumption rate, that has an error level of roughly 30% over both PaSR test configurations. Because QSS assumptions significantly increased the error for this target, better agreement would be obtained by restricting
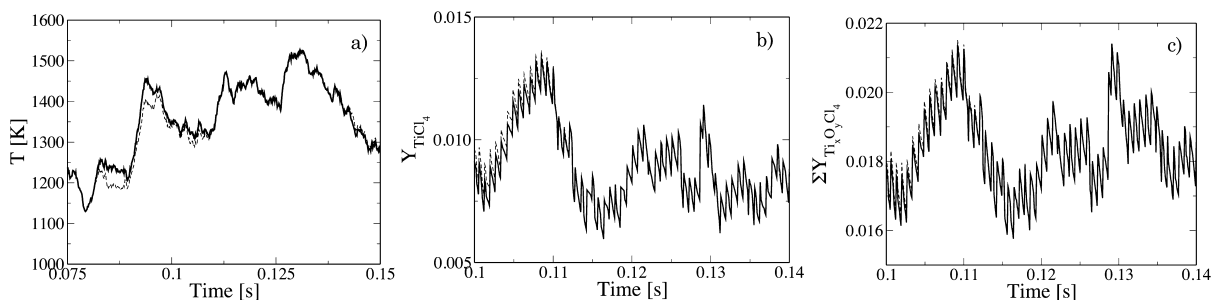
the QSS assumption to non-Ti species. However, it must be pointed out that, in the absence of relevant, quantitative experimental kinetic data to validate the chemistry, there is considerable uncertainty in the original model itself, which should be kept in mind when assessing the validity of the reduced scheme. Figure 4 provides some visualization of the errors reported in Figure 2 for temperature, $TiCl_4$, and $\sum Y_{Ti_xO_yCl_z}$. It can be observed that the temperature predicted by the reduced model follows very closely the detailed solution, except over a short period of time, where T is under-predicted (illustrated in Figure 4a.). No such differences can be found for the Ti species (Figure 4b,c).

To ensure that the reduction procedure did retain an appropriate description of the methane oxidation chemistry, the laminar flame speed of methane/air unstretched premixed flame is computed a posteriori using the reduced models and compared to the detailed predictions in Figure 5. Very good
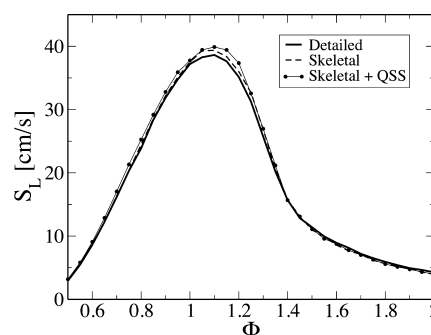

Figure 5. Prediction of methane/air laminar flame speed: comparison between detailed (solid line), 51-species skeletal (dashed line), and 51-species skeletal with quasi-steady state assumption (filled symbols).

agreement is obtained over a wide range of equivalence ratios, with only a small discrepancy observed close to stoichiometry, bringing some confidence that the reduced model can be used in both nonpremixed and premixed configurations.

Figure 6 compares the computational cost of using various models to simulate 10 residence times of the PaSR test configurations. Data have been normalized by the time required by the detailed, 107-species model. Computational cost commonly scales quadratically with the number of species and linearly with the number of reactions. Because the automatic reduction procedure simultaneously removes both species and reactions, a slightly better scaling is observed, with a factor of 5 on the timing obtained by dividing the number of species by two. The introduction of quasi-steady state assumptions contributes to reduce the computational time
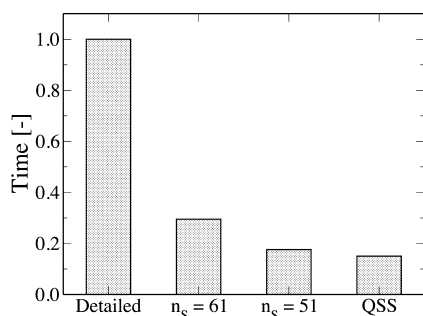

Figure 4. Comparison of actual profiles of temperature and relevant species in the nonpremixed PaSR, obtained using the detailed mechanism (thick lines) and the skeletal + QSS model (dashed line): (a) temperature, (b) $TiCl_4$ mass fraction, (c) $\sum Y_{Ti_xO_yCl_z}$.

Figure 6. Comparison of the computational cost between detailed and reduced models.

required, yet slightly less so than direct species and reaction elimination. However, no transport equation is required for QSS species in CFD simulation, which will lead to additional gains in storage and CPU time.

Finally, both test PaSR are run for five residence times, during which individual reaction rates are integrated. The resulting data can be postprocessed into the flowchart shown in Figure 7, which describes the observed main chemical pathways
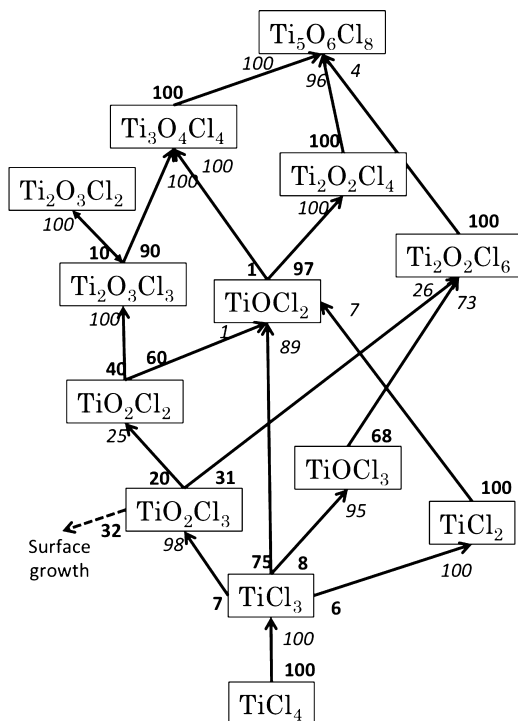

Figure 7. Major chemical pathways in the oxidation of $TiCl_4$ as identified from nonpremixed PaSR results using the skeletal model.

leading from $TiCl_4$ to the nuclei precursor $Ti_5O_6Cl_8$, as described by the simpler, final reduced model. The titanium oxidation process still requires 13 Ti-containing species interacting through 50 reactions. Arrows indicate how Ti atoms get transferred from initial $TiCl_4$ to final $Ti_5O_6Cl_8$. On each arrow going from species A to species B, two numbers can be found. The first one, written in bold, indicates how much of species A gets converted into species B. The second one, in italic, indicates how much of species B comes from species A. Some observations can be made from this graph:

- While the number of reactions involving Ti species is still high, the reduction procedure weeded out a lot of minor interactions between Ti species, allowing for a clear path from $TiCl_4$ to $Ti_5O_6Cl_8$ to emerge, along which the number of Ti atoms in the molecules progressively increases.
- However, this path is not as linear as what is commonly found in reduced models for hydrocarbon combustion, with species interacting significantly with several other species. Each of these interactions are important for the overall production of $Ti_5O_6Cl_8$ precursors and, hence, for the prediction of the nucleation rate. Therefore, no obvious additional simplification of the kinetic model can be done at this point.

Further investigation of the average mass fractions of the various Ti-containing intermediates, shown in Figure 8 for both
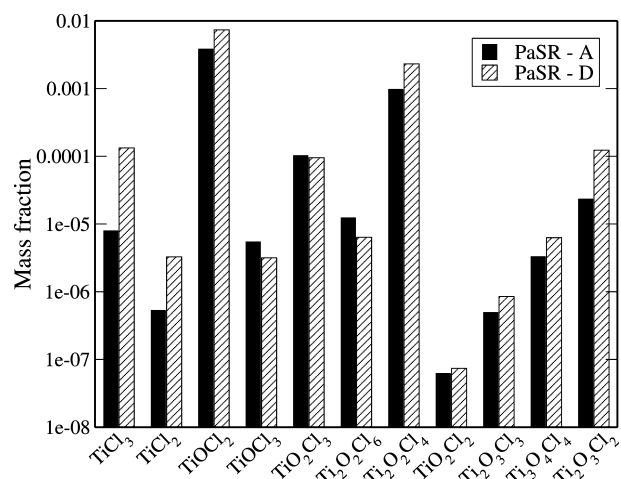

Figure 8. Average mass fraction of Ti-containing intermediate species observed in PaSR—A and PaSR—D simulations.

A and D PaSR configurations, confirms previous observations by Singh[40] that the predominant, stable intermediates are $TiOCl_2$ monomers and $Ti_2O_2Cl_4$ dimers, all other Ti-containing species having mass fractions on average more than an order of magnitude lower than those two species.

■ CONCLUSIONS

Detailed chemistry is thought to be important for modeling TiO_2 nanoparticle synthesis in flame reactors, but due to their typically large sizes, the use of detailed kinetic schemes is prohibitive in turbulent flow solvers using finite-rate chemistry approaches. In this work, we provided a systematic methodology to generate compact chemical models that can still reproduce the key dynamic characteristics of gas-phase titanium oxidation in a hydrocarbon flame predicted using detailed chemistry. Using the simpler partially stirred reactor model as a substitute for more complex turbulent flame configurations, we obtained and validated (using the detailed model as reference) a 36-species model and 237 reaction steps. This reduced mechanism provides a significant computational speed-up compared to the original chemical model. We observed that the titanium oxidation chemistry proposed in the literature[12] can be significantly simplified, up to a point where a clear path from reactant to product emerges. Yet, the number of Ti species in the final model required to maintain the nucleation rate predictions at an acceptable level of accuracy remains

relatively high (10 out of 36) due to the complexity of the interactions between Ti species. We also showed that hydrocarbon chlorination chemistry plays a minor role in the flame dynamics, with only a couple of species retained in the final model. Finally, the reduced model development being for the most part fully automatic, any improvement in Ti kinetic modeling can be reflected quickly in the reduced model, a significant benefit of DRGEP and related techniques over fully manual reduction.

■ ASSOCIATED CONTENT

Ⓢ Supporting Information

List of reactions included in the reduced kinetic mechanism developed in this work. The Supporting Information is available free of charge on the ACS Publications website at DOI: 10.1021/acs.iecr.5b00130.

■ AUTHOR INFORMATION

Corresponding Author
*Phone +1 (607) 254-5281. E-mail: pp427@cornell.edu.

Notes
The authors declare no competing financial interest.

■ ACKNOWLEDGMENTS

■ REFERENCES

(1) Bankmann, M.; Brand, R.; Engler, B.; Ohmer, J. Forming of high surface area TiO₂ to catalyst supports. *Catal. Today* **1992**, *14*, 225−242.

(2) Wang, H.; Wu, Z.; Zhao, W.; Guan, B. Photocatalytic oxidation of nitrogen oxides using TiO₂ loading on woven glass fabric. *Chemosphere* **2007**, *66*, 185−190.

(3) Pratsinis, S. E.; Zhu, W.; Vemury, S. The role of gas mixing in flame synthesis of titania powders. *Powder Technol.* **1996**, *86*, 87−93.

(4) Ukaji, E.; Furusawa, T.; Sato, M.; Suzuki, N. The effect of surface modification with silane coupling agent on suppressing the photo-catalytic activity of fine TiO₂ particles as inorganic UV filter. *Appl. Surf. Sci.* **2007**, *254*, 563−569.

(5) Fujishima, A. Discovery and applications of photocatalysis - Creating a comfortable future by making use of light energy. *Japan Nanonet Bulletin* **2005**, *44*, https://archive.is/29CtP.

(6) Roth, P. Particle synthesis in flames. *Proc. Combust. Inst.* **2007**, *31*, 1773−1788.

(7) Future Markets Inc. *The World Market for Titanium Dioxide Nanopowders*; Annual report; April, 2011.

(8) Raman, V.; Fox, R. O. Modeling of fine-particle formation in turbulent flames. *Annu. Rev. Fluid Mech.* **2016**, *49*, 1−35.

(9) Mehta, M.; Sung, Y.; Raman, V.; Fox, R. O. Multiscale Modeling of TiO₂ Nanoparticle Production in Flame Reactors: Effect of Chemical Mechanism. *Ind. Eng. Chem. Res.* **2010**, *49*, 10663−10673.

(10) Mehta, M.; Raman, V.; Fox, R. O. On the role of gas-phase and surface chemistry in the production of titania nanoparticles in turbulent flames. *Chem. Eng. Sci.* **2013**, *104*, 1003−1018.

(11) West, R. H.; Beran, G. J. O.; Green, W. H.; Kraft, M. First-principles thermochemistry for the production of TiO₂ from TiCl₄. *J. Phys. Chem. A* **2007a**, *111*, 3560−3565.

(12) West, R. H.; Shirley, R. A.; Kraft, M.; Goldsmith, C. F.; Green, W. H. A detailed kinetic model for combustion synthesis of titania from TiCl₄. *Combust. Flame* **2009**, *156*, 1764−1770.

(13) Fox, R. O. *Computational Models for Turbulent Reacting Flows*; Cambridge Series in Chemical Engineering; Cambridge University Press: 2003.

(14) Haworth, D. C.; Pope, S. B. In *Turbulent Combustion*; Echekki, T., Mastorakos, E., Eds.; Springer: 2011.

(15) Hiremath, V.; Lantz, S. R.; Wang, H.; Pope, S. B. Computationally-Efficient and Scalable Parallel Implementation of Chemistry in Simulations of Turbulent Combustion. *Combust. Flame* **2012**, *159*, 3096−3109.

(16) Lu, T.; Law, C. Linear Time Reduction of Large Kinetic Mechanisms With Directed Relation Graph: n-Heptane and Iso-octane. *Combust. Flame* **2006**, *144*, 24−36.

(17) Lu, T.; Law, C. On the Applicability of Directed Relation Graphs to the Reduction of Reaction Mechanisms. *Combust. Flame* **2006**, *146*, 472−483.

(18) Pepiot, P.; Pitsch, H. An efficient error-propagation-based reduction method for large chemical kinetic mechanisms. *Combust. Flame* **2008**, *154*, 67−81.

(19) Niemeyer, K. E.; Sung, C.-J.; Raju, M. P. Skeletal mechanism generation for surrogate fuels using directed relation graph with error propagation and sensitivity analysis. *Combust. Flame* **2010**, *157*, 1760−1770.

(20) Valorani, M.; Creta, F.; Goussis, D. A.; Lee, J. C.; Najm, H. N. An automatic procedure for the simplification of chemical kinetic mechanisms based on CSP. *Combust. Flame* **2006**, *146*, 29−51.

(21) Nagy, T.; Turanyi, T. Reduction of very large reaction mechanisms using methods based on simulation error minimization. *Combust. Flame* **2009**, *156*, 417−428.

(22) Sun, W.; Chen, Z.; Gou, X.; Ju, Y. A path flux analysis method for the reduction of detailed chemical kinetic mechanisms. *Combust. Flame* **2010**, *157*, 1298−1307.

(23) Pepiot, P.; Pitsch, H. A Chemical Lumping Method for the Reduction of Large Chemical Kinetic Mechanisms. *Combust Theory Modell.* **2008**, *12*, 1089−1108.

(24) Ahmed, S. S.; Mauss, F.; Moréac, G.; Zeuch, T. A Comprehensive and Compact n-Heptane Oxidation Model Derived Using Chemical Lumping. *Phys. Chem. Chem. Phys.* **2007**, *9*, 1107−1126.

(25) Huang, H.; Fairweather, M.; Griffiths, J. F.; Tomlin, A. S.; Brad, R. B. A Systematic Lumping Approach for the Reduction of Comprehensive Kinetic Models. *Proc. Combust. Inst.* **2005**, *30*, 1309−1316.

(26) Bodenstein, M.; Lind, S. C. Geschwindigkeit der Bildung des Bromwasserstoffs aus seinen Elementen. *Z. Phys. Chem.* **1906**, *57*, 168.

(27) Chen, J. Y. A general procedure for constructing reduced reaction mechanisms with given independent relations. *Combust. Sci. Technol.* **1988**, *57*, 89−94.

(28) Keck, J. C.; Gillespie, D. Rate-controlled partial-equilibrium method for treating reacting gas-mixtures. *Combust. Flame* **1971**, *17*, 239−264.

(29) Maas, U.; Pope, S. Simplifying Chemical Kinetics: Intrinsic Low-Dimensional Manifolds in Composition Space. *Combust. Flame* **1992**, *88*, 239−264.

(30) Bykov, V.; U, M. The extension of the ILDM concept to reaction-diffusion manifolds. *Combust Theory Modelling* **2007**, *11*, 839−862.

(31) Ren, Z.; Pope, S. B.; Vladimirsky, A.; Guckenheimer, J. M. The invariant constrained equilibrium preimage curve method for the dimension reduction of chemical kinetics. *J. Chem. Phys.* **2006**, *124*, 114111.

(32) Pope, S. B. Computationally efficient implementation of combustion chemistry using in situ adaptive tabulation. *Combust Theory Modell.* **1997**, *1*, 41−63.

(33) Tonse, S. R.; Moriarty, N. W.; Brown, N. J.; Frenklach, M. PRISM: Piecewise reusable implementation of solution mapping. An economical strategy for chemical kinetics. *Israel J. Chem.* **1999**, *39*, 97−106.

(34) Ren, Z.; Pope, S. B. An investigation of the performance of turbulent mixing models. *Combust. Flame* **2004**, *136*, 208−216.

(35) Bowman, C.; Hanson, R.; Davidson, D.; Gardiner, W.Jr.; Lissianski, V.; Smith, G.; Golden, D.; Frenklach, M.; Goldenberg, M. GRI-Mech2.11; http://www.me.berkeley.edu/gri_mech/.

(36) Shah, J. J.; Fox, R. O. Computational fluid dynamics simulation of chemical reactors: Application of in situ adaptive tabulation to methane thermochlorination chemistry. *Ind. Eng. Chem. Res.* **1999**, *38*, 4200−4212.

(37) Shirley, R. A.; Akroyd, J.; Miller, L. A.; Inderwildi, O. R.; Riedel, U.; Kraft, M. Theoretical insights into the surface growth of rutile TiOl$_2$. *Combust. Flame* **2011**, *158*, 1868−1876.

(38) Hiremath, V.; Pope, S.; Ren, Z. Combined dimension reduction and tabulation strategy using ISAT-RCCE-GALI for the efficient implementation of combustion chemistry. *Combust. Flame* **2011**, *158*, 2113−2127.

(39) Pepiot, P. Automatic strategies to model transportation fuel surrogates Ph.D. thesis, Department of Mechanical Engineering, Stanford University, 2008.

(40) Singh, R. I. Direct Numerical Simulation and Reaction Path Analysis of Titania Formation in Flame Synthesis. Master of Science in Engineering Thesis, University of Texas at Austin, 2012.